

Space-time optimized table lookup

THOMAS HÄNER*, Microsoft, Switzerland
VADYM KLIUCHNIKOV, Microsoft, Canada
MARTIN ROETTELER, Microsoft, United States
MATHIAS SOEKEN, Microsoft, Switzerland

We describe a space-time optimized circuit for the table lookup subroutine from lattice-surgery surface code primitives respecting 2D grid connectivity. Table lookup circuits are ubiquitous in quantum computing, allowing the presented circuit to be used for applications ranging from cryptography to quantum chemistry. Surface code is the leading approach to scalable fault-tolerant quantum computing pursued by industry and academia. We abstract away surface code implementation details by using a minimal set of operations supported by the surface code via lattice-surgery. Our exposition is accessible to a reader not familiar with surface codes and fault-tolerant quantum computing.

1 INTRODUCTION

For certain computational tasks, quantum computers are known to asymptotically outperform traditional computers running state-of-the-art algorithms. This includes factoring [Shor 1997] and simulating systems that must be treated quantum mechanically to achieve the desired accuracy [von Burg et al. 2021]. To assess whether an asymptotic speedup translates to a computational advantage *in practice*, a quantum algorithm must be broken down into elementary operations for which runtime estimates can be derived from the chosen error correction protocol. Promising applications can then be optimized to reduce the resource requirements (qubits and time) further. In turn, this reduces the time until the given quantum algorithm can be used to achieve a quantum advantage at application scale.

Over the recent years, promising quantum algorithms for applications such as factoring and simulating quantum chemistry have been optimized significantly [Gidney and Ekerå 2019; Häner et al. 2020; Lee et al. 2021; von Burg et al. 2021]. To this end, researchers have explored various tradeoffs (e.g., space for time) in order to reduce the many overheads that must be introduced to achieve a fault-tolerant implementation.

The table lookup is one subroutine that can be used to reduce the resource requirements for state preparation [Low et al. 2018] and arithmetic [Gidney and Ekerå 2019]. As such, it is used in state-of-the-art implementations of both Shor’s algorithm for factoring and computing discrete logarithms [Gidney and Ekerå 2019; Häner et al. 2020] and algorithms for solving chemistry problems [Lee et al. 2021; von Burg et al. 2021]. Given this broad range of applications, it makes sense to manually optimize this subroutine, including a detailed layout for execution based on lattice-surgery surface code. We explore various implementation tradeoffs and assess their impact on the total physical space/time volume under different assumptions regarding the fault-tolerance protocol and qubit quality.

The paper is structured as follows. The next section introduces the table logic operation on a logical level. Section 3 describes how to map the state-of-the-art table lookup construction for table lookup to surface code and derives general cost estimates in terms of qubit count logical compute cycle count. Section 4 proposes a new construction that allows to reduce the compute cycle count by using more qubits. Section 5 describes several universally useful gadgets that are used throughout the paper.

*This work was completed prior to T.H. joining AWS

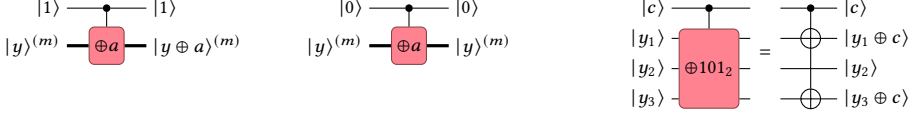


Fig. 1. CXOR gates. A bold line represents a multi-qubit register, in which the (m) suffix to a qubit register denotes the number of bits in the register.

2 TABLE LOOKUP

Here, we briefly introduce the basic quantum operations (gates) that we use to implement table lookup. For a thorough introduction to quantum computing, we refer the reader to the textbook by Nielsen and Chuang [Nielsen and Chuang 2000].

The controlled NOT or CNOT gate, with the first qubit acting as the control qubit, is defined as

$$|c\rangle|t\rangle \mapsto |c\rangle|t \oplus c\rangle, \quad (1)$$

and the multi-target CNOT gate is defined as

$$|c\rangle|t_1\rangle \dots |t_m\rangle \mapsto |c\rangle|t_1 \oplus c\rangle \dots |t_m \oplus c\rangle, \quad (2)$$

where we use ‘ \oplus ’ to denote both Boolean and bitwise XOR.

Given K bit strings d_0, \dots, d_{K-1} , each of length m , a table lookup with $k \geq \lceil \log_2 K \rceil$ input qubits $|x\rangle = |x_1 \dots x_k\rangle$ and m output qubits $|y\rangle = |y_1 \dots y_m\rangle$ maps

$$|x\rangle|y\rangle \mapsto |x\rangle|y \oplus f(x)\rangle, \quad (3)$$

where $f(x_1, \dots, x_k) = d_x$, if $x = (x_1 \dots x_k)_2 < K$, and an arbitrarily chosen output if $x \geq K$ [Babbush et al. 2018] (for optimization purposes). In the input assignment, x_1 is the most significant bit. We assume that the circuit will never be run on undefined inputs, or that undefined outputs do not negatively affect the overall algorithm. For $K = 1$ and $k = 0$ input qubits, the function f turns into the constant bit string d_0 , and the definition becomes $|y\rangle \mapsto |y \oplus d_0\rangle$. We say that d_0 is the *data being looked up* by the table lookup circuit. The controlled table lookup function is defined similarly with an additional control qubit $|c\rangle$.

$$|c\rangle|x\rangle|y\rangle \mapsto |c\rangle|x\rangle|c ? y \oplus f(x) : y\rangle, \quad (4)$$

where the ‘ $\cdot ? \cdot : \cdot$ ’ denotes the *if-then-else* operation.

The unary-iterate table lookup construction [Babbush et al. 2018] requires $O(K)$ T gates, in particular, the number does not depend on the number of output bits [Babbush et al. 2018]. We will first illustrate the construction for a single input, i.e., $k = 1$, and then derive a recursive construction for the general case.

One-input table lookup. For any bit string a of length m , the bitwise XOR operation maps

$$|y\rangle \mapsto |y \oplus a\rangle, \quad (5)$$

where $|y\rangle$ is an m -qubit computational basis state. One can think of this operation as a table lookup with zero inputs. Similarly, its controlled version can be seen as a controlled table lookup with zero inputs

$$|c\rangle|y\rangle \mapsto |c\rangle|c ? y \oplus a : y\rangle. \quad (6)$$

This controlled bitwise XOR operation, called CXOR, can be implemented using multi-target CNOT gates, see Figure 1.

Space-time optimized table lookup



Fig. 2. AND and AND[†] gates. Each of the variables c_1, c_2 is represented by a single qubit.

A one-input table lookup for two bit strings d_0 and d_1 than can be implemented as

$$\begin{array}{c}
 |x\rangle \text{---} \oplus \text{---} |x\rangle \\
 |y\rangle^{(m)} \text{---} \oplus d_0 \text{---} \oplus d_1 \text{---} |y \oplus d_x\rangle^{(m)}
 \end{array} \quad (7)$$

for a function $f : \{0, 1\} \rightarrow \{0, 1\}^m$. The bold line and (m) -suffix represent an m -qubit register and the output is any bit string of length m . Note that a one-input table lookup circuit requires only Clifford operations and a zero-input table lookup requires only Pauli gates.

To make an efficient circuit for a controlled one-input table lookup, we make use of AND and AND[†] gates as defined in Figure 2. We use the shorthand $c_1 c_2$ to denote the AND of the bits c_1 and c_2 . Note that the AND gate requires four $|T\rangle$ magic states or one $|CCZ\rangle$ magic state, whereas AND[†] requires only Clifford operations. Note how the AND gate in Figure 2 is expressed in terms of a CCiX gate and an S gate on the target qubits.

Using one AND and one AND[†] gate, the controlled one-input table lookup can be implemented as

$$\begin{array}{c}
 |c\rangle \text{---} \text{---} |c\rangle \\
 |x\rangle \text{---} \text{---} |x\rangle \\
 |y\rangle^{(m)} \text{---} \oplus d_0 \text{---} \oplus d_1 \text{---} |c ? y \oplus d_x : y\rangle^{(m)}
 \end{array} \quad (8)$$

where $f : \{0, 1\} \rightarrow \{0, 1\}^m$. The first CXOR gate is executed when $|c\rangle$ is one and $|x\rangle$ is zero. The second CXOR gate is executed when both $|c\rangle$ and $|x\rangle$ are one.

Recursive construction. It is more convenient to first construct a *controlled* table lookup recursively to then use this construction to arrive at an implementation of a non-controlled table lookup.

The controlled table lookup construction for K bit strings d_0, \dots, d_{K-1} and $k = \lceil \log_2 K \rceil$ inputs is depicted in Figure 3a. Based on the controlled one-input table lookup in Eq. (8), we construct a controlled k -input table lookup by splitting the bit strings into two sets, the first one containing the first 2^{k-1} bit strings, and the second one containing the rest. Note that the first set is addressed when the most-significant bit x_1 is 0, and the second set is addressed when x_1 is 1. This corresponds to the two co-factors $f(0, x_2, \dots, x_k)$ and $f(1, x_2, \dots, x_k)$ of f . The input register in the second controlled table lookup in Figure 3a on the right-hand side might require fewer than $k - 1$ inputs.

Figure 3b shows how to combine two controlled $(k - 1)$ -input table lookup circuits to arrive at a k -input table lookup circuit. We first apply the negatively controlled version to look up all bit strings at addresses starting with zero and then we apply the controlled version to look up all bit strings at addresses starting with a one. Note that we could also switch the order of negatively and positively controlled table lookup circuits. We will show later that they can also be run in parallel to increase the magic state consumption rate and the utilization of output qubits.

Magic state requirements. Let $N_{\text{AND}}^{\text{TL}}(k)$ be the number of AND gates used by table lookup with k inputs and $N_{\text{AND}}^{\text{CTL}}(k)$ be the number of AND gates used by controlled table lookup with k inputs.

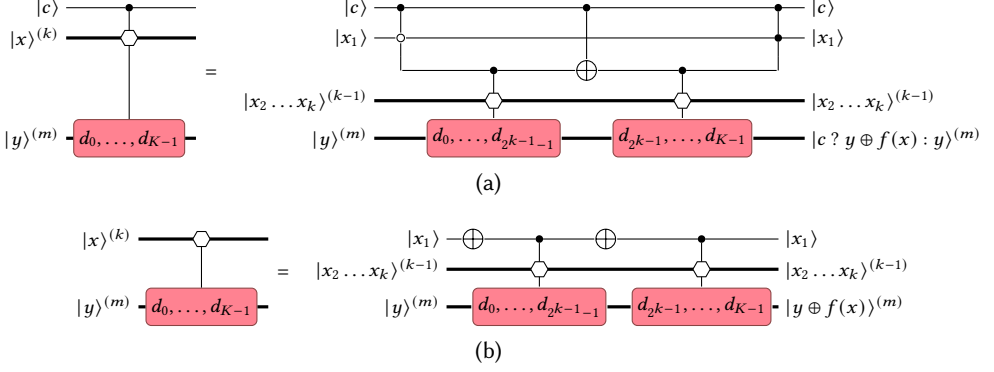


Fig. 3. (a) controlled and (b) uncontrolled k -input and m -output table lookup circuit; we use a hexagon to denote the input register for the table lookup.

Then we have the following:

$$N_{\text{AND}}^{\text{TL}}(k) = 2N_{\text{AND}}^{\text{CTL}}(k-1) \quad (9)$$

$$N_{\text{AND}}^{\text{CTL}}(0) = 0 \quad (10)$$

$$N_{\text{AND}}^{\text{CTL}}(1) = 1 \quad (11)$$

$$N_{\text{AND}}^{\text{CTL}}(k) = 1 + 2N_{\text{AND}}^{\text{CTL}}(k-1) = 2^k - 1, \text{ for } k \geq 0 \quad (12)$$

$$N_{\text{AND}}^{\text{TL}}(k) = 2 \cdot (2^{k-1} - 1) = 2^k - 2, \text{ for } k \geq 1 \quad (13)$$

$$N_{\text{AND}}^{\text{TL}}(0) = 0 \quad (14)$$

Therefore the number of T states required by unary-iterate table lookup is

$$N_{\text{T}}^{\text{TL}}(k) = 4(2^k - 2) = 2^{k+2} - 8, \text{ for } k \geq 1 \quad (15)$$

$$N_{\text{T}}^{\text{TL}}(0) = 0 \quad (16)$$

3 MAPPING TO LATTICE-SURGERY SURFACE CODE

The goal of this section is to describe an explicit mapping of table lookup to lattice surgery operations on logical qubits in a 2D grid. We do this by using the basic operations given in [Table 1](#) and assuming the availability of $|S\rangle$ - and $|T\rangle$ -states. We also use these operations to construct more high-level gadgets described in [Section 5](#).

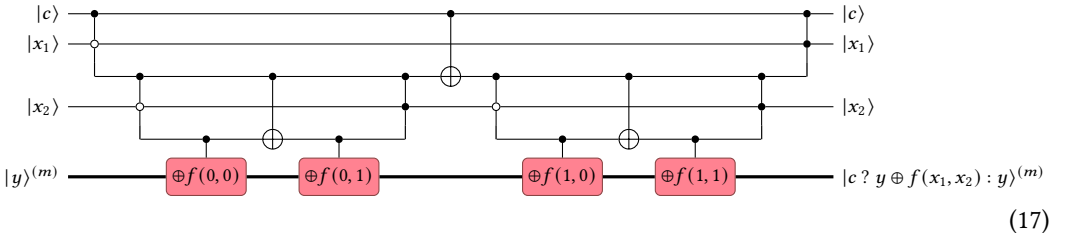
We start by applying several circuit transformations and optimizations to the table lookup circuit. Some of the circuit gadgets used in this section are described in detail in [Section 5](#).

Table 1. Operations supported by surface codes with lattice surgery and restrictions on them. Gray circles indicate that operation uses neighbouring qubits; the qubits start and end in a “blank” state.

Symbol	Name	Remarks
Circuit	2D	
	Measure Z	Leaves qubit in a “blank” state
	Measure X	Leaves qubit in a “blank” state
	Prepare $ 0\rangle$	Expects qubit in a “blank” state
	Prepare $ +\rangle$	Expects qubit in a “blank” state
	Measure ZZ	Vertical only
	Measure XX	Horizontal only
	Measure XZ	Blocks neighbors; expects and leaves them in “blank” state

3.1 Surface-code specific optimizations and gadgets

Let us start with an explicit example of a controlled table lookup circuit with $k = 2$ input and m output bits, which follows from Figure 3a and (8):



We rewrite AND gates in terms of C*C*iX and *S* gates as described in Figure 2 and AND[†] in terms of *X* measurement and classically controlled CZ gates. We move the *S* gates past the controls of CXOR and C*C*iX gates as shown in Figure 4. Then, we further replace *S* gates with the joint measurement-based $|S\rangle$ -state injection circuit shown in Figure 5(a)¹ and classically-controlled CZ gates with the delayed-choice CZ gadget [Gidney and Fowler 2019a] depicted in Figure 6(a). In this gadget, the measurement gates on the top two qubits measure in the *Z*-basis if the measurement result a is 1, and in the *X*-basis otherwise. The “Prepare $|CZ\rangle$ ” gadget is depicted in Figure 6(b) and can be executed before the measurement result a is known. We also implement C*C*iX gates with the fast C*C*iX gadget illustrated in Figure 7 and described in Section 5.2. CXOR gates that are followed by *S* gates (highlighted by blue rectangles in Figure 4) are implemented using the multi-target CNOT gate as illustrated in Figure 8 making use of the $|S\rangle$ -state injection circuit from Figure 5(b).

¹This step can likely be simplified by directly implementing *S* gates in surface code as described in [Bombin et al. 2021].

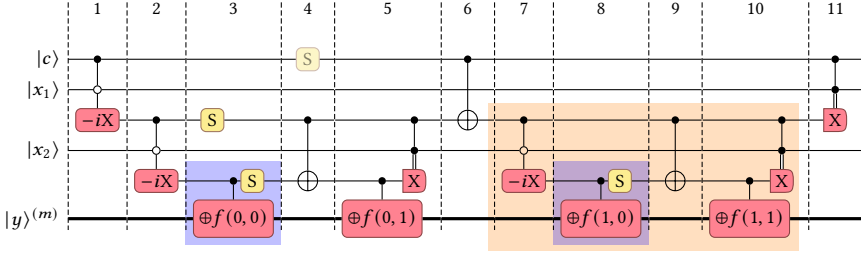


Fig. 4. Expanded two-input controlled table lookup circuit. The circuit follows from (17) and Figure 2. Register $|c\rangle$ is the control bit, $|x_1\rangle$ and $|x_2\rangle$ are two input bits. We will show that gates in blue areas can be executed simultaneously. The semi-transparent S gate is not present for the two input table lookup, but will be present when the circuit is a part of table lookup with more inputs. Dashed lines indicate layers of gates that are implemented simultaneously. The orange area highlights a controlled table lookup circuit with one input.

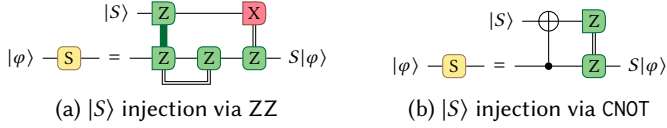


Fig. 5. These circuits apply an S operation to a qubit by consuming and injecting an $|S\rangle$ state.

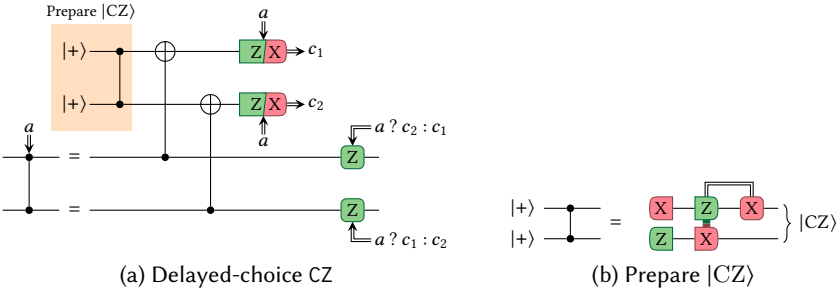


Fig. 6. The delayed-choice CZ operation conditionally applies a CZ operation on measurement result a and therefore can be used to implement AND^\dagger . The “Prepare $|CZ\rangle$ ” operation can be performed before the measurement result is known.

3.2 Logical cycles estimates

We are ready to determine the number of logical cycles required by the unary-iterate table lookup circuit. We base our estimates on the duration (number of logical cycles) of the following commonly-used operations:

- τ_{RCX} : time of remote CNOT gate along an arbitrary path of qubits
 - τ_{RZZ} : time of remote ZZ measurement along an arbitrary path of qubits
 - τ_{RXZ} : time of remote XZ measurement along an arbitrary path of qubits
 - τ_{CXOR} : total time of CXOR
 - τ_{CAT} : cat state initiation time in CXOR implementation
- (18)

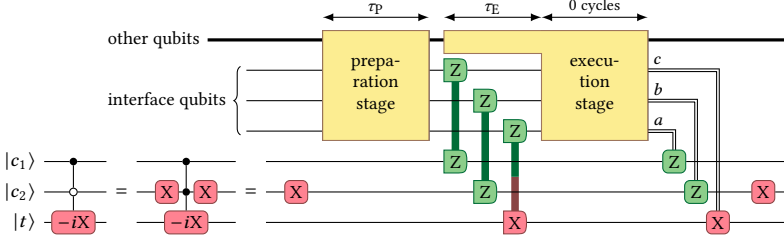


Fig. 7. High-level view of CCiX gadget. The CCiX gadget described in Section 5.2 consist of three parts: a preparation stage at which $|T\rangle$ states are consumed and $|S\rangle$ states are cloned, three parallel remote joint measurements, and a short execution stage. Clifford operation can be performed on the target qubits right after the remote joint measurements. To apply non-Clifford operations we need to wait for the execution stage to complete and resolve Pauli corrections.

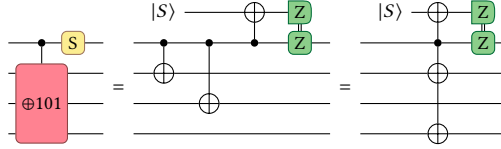


Fig. 8. CXOR and S implemented via one multi-target CNOT. CNOTs sharing the same control are merged into a single multi-target CNOT gates that can be executed in constant time independent on the number of targets.

We further assume that X and Z measurements as well as X and Z corrections take no time. We can now discuss in detail the timing of the layers in Figure 4, taking into account all introduced optimizations.

Layers 1, 2, and 7 (Total time: τ_{RZZ}). The time for executing the fast CCiX gadget is dominated by the three remote ZZ and XZ measurements that are shown in Figure 7. The preparation stage can always be moved to previous layers if we use two fast remote CCiX gadgets that we alternate between calls. For example, the first CCiX gadget is used in layer 1, while the second one is used in layer 2, and so on. Typically XZ measurements take longer than ZZ measurements. However a small part of the XZ measurement that prepares a Hadamard-conjugated Bell pair can be done slightly earlier. Consequently, most of the qubits involved in an XZ or ZZ measurement are occupied for τ_{RZZ} logical cycles. To avoid delays due to Pauli corrections that depend on yet unknown measurement outcomes, we require that the execution stage of the fast CCiX gadget uses fewer logical cycles than a remote measurement, i.e., $\tau_E \leq \tau_{RZZ}$.

Layer 3 (Total time: $\max(\tau_{RZZ}, \tau_{CAT})$). A part of the multi-target CNOT gate can be moved to the next layer, and only the cat state preparation stage needs to be accounted for in this layer (see supplemental material). At the same time we apply an S gate via $|S\rangle$ -state injection using the circuit in Figure 5(a), which requires τ_{RZZ} execution cycles. The duration of this layer can therefore be upper bounded by the maximal duration of these two operations.

Layers 4, 6, and 9 (Total time: τ_{RCX}). We use the fastest circuit for $|S\rangle$ -state injection and can therefore assume that the execution time is at most that of a remote CNOT operation.

Layers 5 and 10 (Total time: $\max(\tau_{CXOR}, \tau_{RCX})$). We make use of the delayed-choice CZ gate depicted in Figure 6. The $|CZ\rangle$ preparation can be executed in previous layers and the two CNOT gates in the delayed-choice CZ operation can be executed in parallel together with the CXOR gate.

However, because its control is followed by an X measurement, its outcome must be determined immediately, and therefore we account for the full execution time of the CXOR gate.

Layer 8: (τ_{CAT}). This is similar to layer 3, but no S gates are executed.

Layer 11: (τ_{RCX}). The cost is dominated by the CNOT operations in the delayed-choice CZ gate. Under the right conditions, this layer can potentially be executed in the same time as the previous one; however, it is not clear how long of a ladder of dependent AND^\dagger gates can be executed simultaneously. We thus opt for a conservative estimate.

Let us define

$$\tau_R = \max(\tau_{\text{RCX}}, \tau_{\text{RZZ}}, \tau_{\text{CAT}}) \quad (19)$$

$$\tau_M = \max(\tau_{\text{RCX}}, \tau_{\text{CXOR}}) \quad (20)$$

Typically, the cycle times over which we are taking the maximum are equal. It is also typically the case that $\tau_{\text{CXOR}} \geq \tau_{\text{RCX}}$. Therefore we can assume $\tau_R = \tau_{\text{RCX}}$ and $\tau_M = \tau_{\text{CXOR}}$ in practice. Using this notation, we can bound the number of logical cycles for a controlled table lookup with k inputs as $\tau_{\text{CTL}}(k)$. In the base case, we have

$$\tau_{\text{CTL}}(1) \leq 3\tau_R + \tau_M, \quad (21)$$

where layers 7–9 each contribute τ_R and layer 10 contributes τ_M (orange rectangle in Figure 4) to the total delay. From the recursive construction in (8), we derive

$$\tau_{\text{CTL}}(k) \leq 3\tau_R + 2\tau_{\text{CTL}}(k-1), \quad \text{for } k \geq 2, \quad (22)$$

where layers 1, 6, and 11 each incur a delay of τ_R . Together with (21) we can derive the closed form expression

$$\tau_{\text{CTL}}(k) \leq 2^{k-1}(6\tau_R + \tau_M) - 3\tau_R, \quad \text{for } k \geq 1. \quad (23)$$

The number of logical cycles needed for uncontrolled table lookup $\tau_{\text{TL}}(k)$ is

$$\tau_{\text{TL}}(k) = 2\tau_{\text{CTL}}(k-1), \quad \tau_{\text{TL}}(1) = 2\tau_M. \quad (24)$$

We note that these estimates assume that we have enough ancillary qubits to perform all remote operations within any given layer simultaneously, and that a ratio of logical qubits to algorithm qubits of 4 : 1 is sufficient for this purpose.

3.3 Number of logical qubits used

The number of abstract qubits used by controlled table lookup with k inputs and m outputs is $2k + m + 1$, 2 qubits per input bit, 1 qubit per output bit, and 1 control qubit. The number of logical qubits needed for table lookup is

$$\sigma_{\text{CTL}}(k) = 4 \cdot (2k + 1) + O(\sqrt{k}) + 2 \cdot m + O(\sqrt{m}) + O(1) \quad (25)$$

The constant term is the number of qubits required for the CCiX and delayed-choice CZ gadgets, qubits for $|S\rangle$ -state delivery and some additional padding qubits to fit the input qubits in a square shape. The number of output qubits is multiplied by 2 corresponding to the number of logical qubits per target in the CXOR gadget as explained in supplemental material. We assume that the target qubits are aligned in a square shape and use a dedicated routine to create a cat state in every second column of that square following a snake like path. This incurs an overhead of at most $O(\sqrt{m})$ additional qubits. The number of the other abstract qubits (control qubit, input qubits, and helper qubits) is multiplied by four to ensure that all layers described in the previous subsection can be executed as fast as possible. To ensure that we can route the remote measurements efficiently from

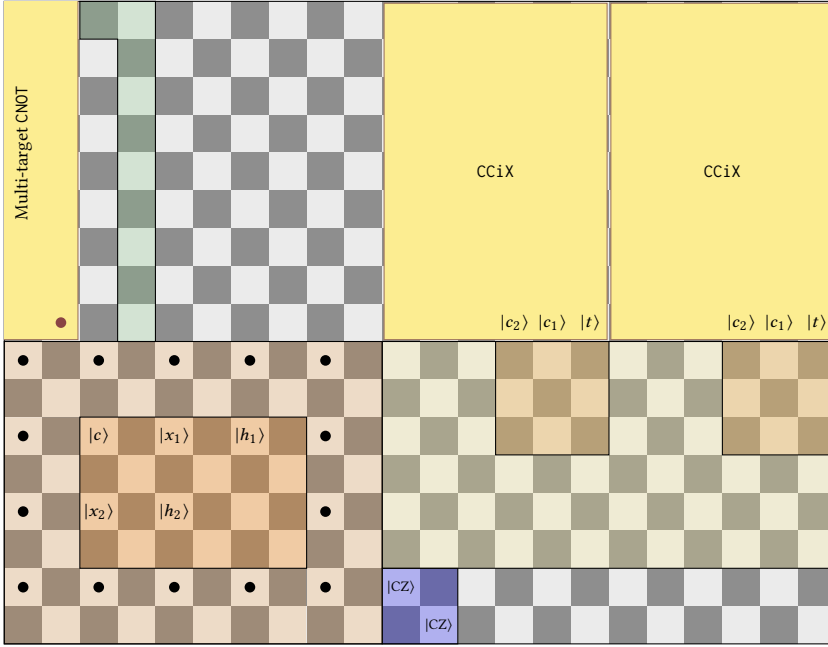



Fig. 9. Arrangement of input qubits, output qubits and gadgets for a controlled 2-input table lookup instance with 2 CCiX gadgets.

these input qubits to the CCiX gadgets we align them in a squarish shape and also use the qubits at the boundary of that shape as auxiliary qubits, which results in the $O(\sqrt{k})$ term in (25).

The number of CCiX gadgets and delayed-choice CZ gadgets is constant and is calculated based on duration of the gadgets and remote ZZ measurement. We need to make sure that consecutive dependent CCiX or delayed-choice CZ gates can be executed without delays (as, e.g., in layers 1 and 2 in Figure 4). The number of qubits required for uncontrolled table lookup on k qubits is the same as the number of qubits for controlled table lookup on $k - 1$ qubits, since we use the control qubit for the most-significant bit:

$$\sigma_{\text{TL}}(k) = \sigma_{\text{CTL}}(k - 1) \quad (26)$$

Layout. Figure 9 provides an overview of the layout, illustrated for a controlled table lookup instance using 2 input bits, 2 CCiX gadgets, and 1 delayed-choice CZ gate. For the $2k + 1$ input qubits and control qubit we use a 4:1 ratio of auxiliary qubits, i.e., for each data qubit there are 3 auxiliary qubits. These are placed in patches of 2×2 qubits , where each data qubit is in the top-left corner. All these patches are aligned in a square shape region and also the boundary around this square shape of 2×2 patches with 1 data qubits and 3 auxiliary qubits is reserved for routing. This region is highlighted in orange in Figure 9 (dark orange for the input qubits and a bit lighter orange for the boundary). The black dots in the boundary are assumed to be some data qubits which may be in a non-blank state but do not require their auxiliary qubits during the execution of the table lookup operation.

The output qubits are part of the CXOR gadget in the top-left corner. The dot in the bottom right is the interface qubit to establish the remote ZZ measurement to initiate the fanout as described in supplemental material. We also assume that all output qubits are arranged in a square with the cat

state arranged in a snake pattern. Some auxiliary qubits are required for the holes in the cat state at the corner of the snake pattern. However, these won't exceed $4\sqrt{m}$ qubits.

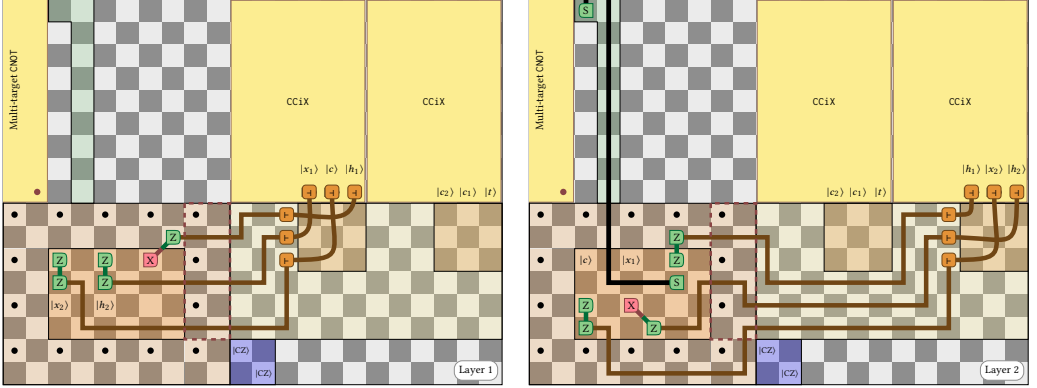
The two CCiX gadgets are located at the top-right in Figure 9. Each spans 9×6 qubits, as described in Section 5.2. Below the CCiX gadgets and right of the input qubits, there is an area of 6×12 qubits, highlighted in yellow, that is used to connect input qubits to the interface qubits of the CCiX gadgets (dots in the lower left corner) via joint ZZ and XZ measurements and teleportation circuits. We will always route these remote measurements through the top 3 qubit patches in the right boundary of the input qubit region. In order to account for permutations of the target and control qubits in the CCiX gadgets, we make use of a 3×3 switch board below each CCiX gadget as described in Section 5.1.

The 9 qubits highlighted in green above the input qubit region is to deliver $|S\rangle$ -states into the input qubit region. Finally, the 2×2 qubits highlighted in blue will contain $|CZ\rangle$ states to execute delayed-choice CZ gates. Following this layout, we can state (25) more precisely as

$$\sigma_{\text{CTL}}(k) = 4(c+2)(r+2) + 90 \cdot \#\text{CCiX} + 4 \cdot \#\text{CZ} + 2m + O(\sqrt{m}), \quad (27)$$

where $c = \lceil \sqrt{2k+1} \rceil$ and $r = \lceil \frac{2k+1}{c} \rceil$ are the number of columns and rows to fit the $2k+1$ input qubits into a square shape, and $\#\text{CCiX}$ and $\#\text{CZ}$ are the number of CCiX and CZ gadgets, respectively.

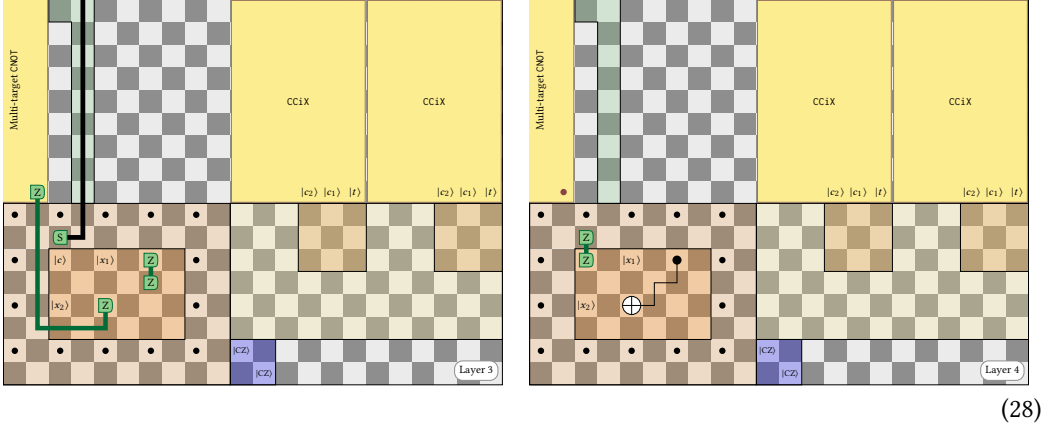
Layer execution. Next, we describe how the operations in each layer in Figure 4 are executed using the layout in Figure 9. The first two layers execute the CCiX gates. Recall that the preparation stages of the CCiX gates can be done in previous layers.



During the preparation stage of the CCiX gates, also the teleportation circuits in the switch boards are performed (see (35)). We then execute the remote joint measurements using more teleportation circuits using remote Measure ZZ & Move operation (see Section 5) together with joint ZZ and XZ measurements for the control lines and the target line, respectively. The brown lines between the teleportation targets in the switch board and the joint measurements are also teleportation circuits. The joint measurements can be executed at the same time as these. We alternate between the CCiX gadgets such that the preparation stages do not interfere. The routing of the teleportation paths between the joint measurements and the switch board is done in a way that the paths always exit in the top three 2×2 qubit patches of the boundary (the dashed rectangle). The measurement in the top patch connects to the top-most qubit in the switch board, whereas the measurement in the bottom patch connects to the bottom-most qubit in the switch board. To route them in parallel, we need three rows of qubit patches as in Layer 1, or four rows of qubit patches if additionally an $|S\rangle$ -state needs to be delivered as in Layer 2 for the injection circuit in the next layer. Because there

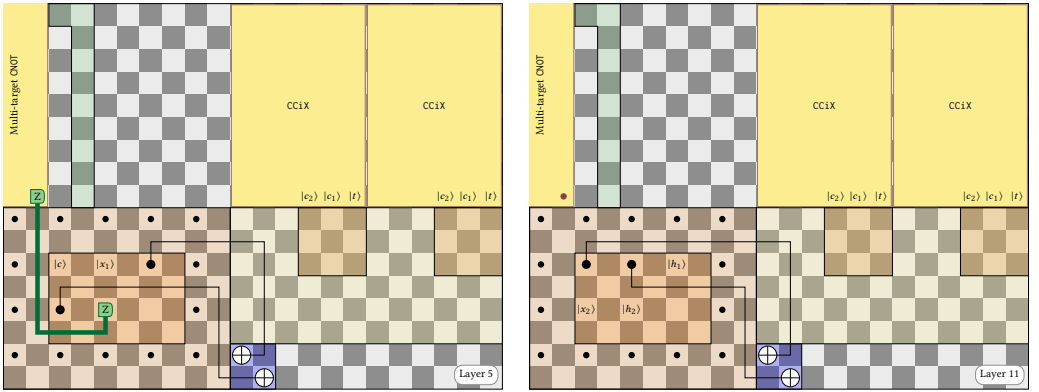
are 6 rows of helper qubits below the CCiX gadgets, teleportation paths can be routed along switch board gadgets when CCiX gadgets further to the right are addressed, as shown in Layer 2.

Layer 3 will use two $|S\rangle$ -states that are prepared in Layer 2. One is for the S gate on $|h_2\rangle$, which is executed together with the CXOR gate as described in Figure 8, and the other one on qubit $|h_1\rangle$, which is prepared below it, such that we can use the $|S\rangle$ injection circuit that uses joint ZZ measurement (see Figure 5(a)). In Layer 3, we execute the CXOR gate by performing a remote joint ZZ measurement with its interface qubit. The $|S\rangle$ is consumed to apply an S gate on $|h_1\rangle$ and optionally another $|S\rangle$ -state is delivered right above $|c\rangle$ in case it needs to be applied in Layer 4.



In Layer 4, if the S gate is applied, it injects the $|S\rangle$ -state via joint ZZ measurement; it also executes a remote CNOT gate controlled on $|h_1\rangle$ targeted on $|h_2\rangle$. Due to the 2×2 patches, a route can readily be found.

Layer 5 executes another CXOR gate as in Layer 3 and also connects the two control qubits $|h_1\rangle$ and $|h_2\rangle$ of the AND^\dagger operation to the $|CZ\rangle$ states via two remote CNOT operations to perform the delayed-choice CZ gate. These are routed such that they exit the input area via the topmost patch and the fourth patch from the top at the right boundary. Recall that the $|CZ\rangle$ states are prepared in previous layers. Layers 6–10 are similar to Layers 1–5 and Layer 11 is another example of a delayed-choice CZ gate.



3.4 T state consumption rate

The highest consumption rate of $|T\rangle$ -states happens during the execution of consecutive CCiX gates (as, e.g., in the first two layers in Figure 4). It is reasonable to average out the consumption rate

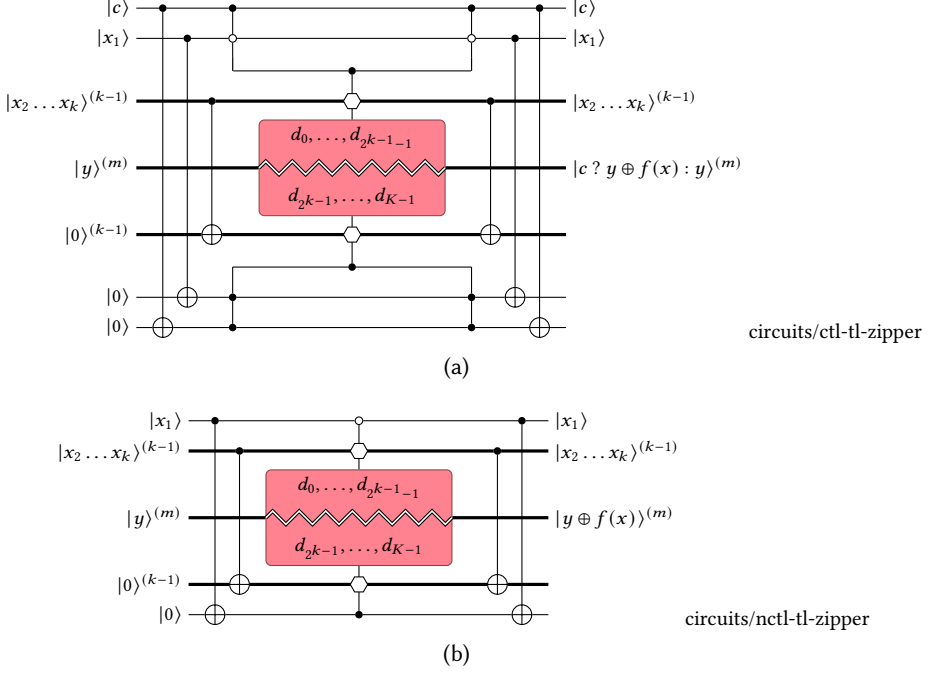


Fig. 10. parallel (a) controlled and (b) uncontrolled k -input and m -output table lookup circuit; we use a hexagon to denote the input register for the table lookup. The idea is to interleave the CXOR gates in each table lookup instance

over a small window of logical cycles using small T -state buffers. The smoothed-out peak number of required $|T\rangle$ -states per cycle is:

$$\frac{\text{Number of T states per CC-iX}}{\tau_{\text{RZZ}}} = \frac{4}{\tau_{\text{RZZ}}} \quad (29)$$

When running several instances of this circuit in parallel we simply multiply the required rate by the number of circuits running in parallel.

4 SPACE-TIME TRADE-OFFS

In this section, we describe optimizations that allow for space-time trade-offs. The zipper construction copies all input qubits $p > 1$ times using the fanout gadget and performs p table lookups simultaneously. Depending on the number of output qubits and p , it may make sense to use separate output registers for the p simultaneous table lookups, merging the outputs into a single register only once both lookups have completed (using CXOR gates). In the case of a large number of output qubits, the two table lookups may write into the same output register by interleaving the execution of the CXOR gates that write to the output register. In the following description, we choose the latter approach and $p = 2$.

4.1 Zipper construction

Figure 10 illustrates the zipper construction for both controlled and uncontrolled table lookup on k input bits and K entries. Fanout gadgets copy all input qubits. Then the upper part writes entries

Space-time optimized table lookup

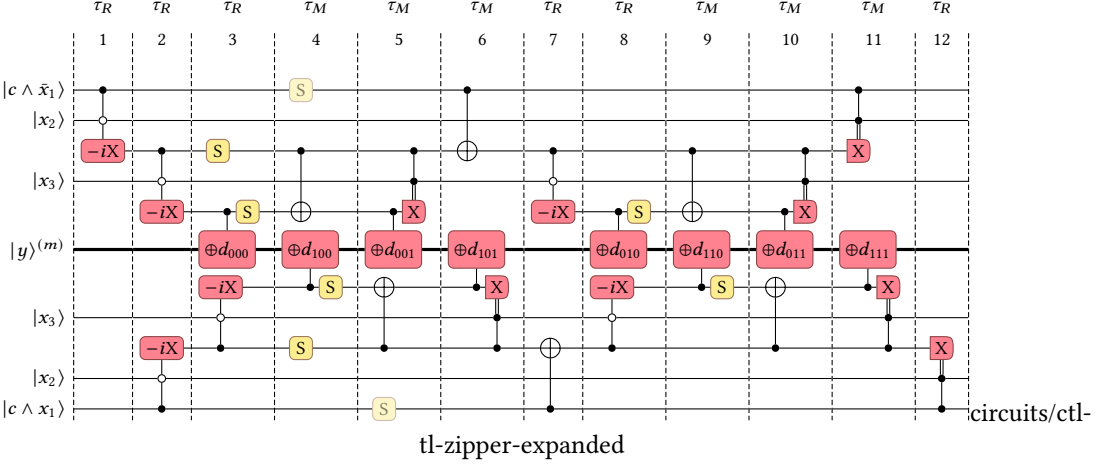


Fig. 11. Similar to Figure 4, we show an expansion of operations assigned to different layers. Here two instances are executed in parallel using the zipper construction. Note how the lower instance is shifted by one layer and how the CXOR gates alternate.

d_x for which the most-significant bit $x_1 = 0$ in the index x , whereas the lower part writes entries for which $x_1 = 1$. Both table lookups share the same target qubit register $|y\rangle$ but no other qubits. The idea is to alternate and interleave the executions of CXOR gates, while executing the other operations in parallel as they act on independent qubits. The controlled table lookup in Figure 10a and the uncontrolled table lookup in Figure 10b are very similar except for the copying of input qubits. Also note that the controlled zipper construction requires one more AND gate compared to the standard construction in Figure 3a.

Figure 11 illustrates the interleaving when $k = 3$, split on x_1 and data lookups for x_2 and x_3 interleaved. Note that the construction requires one more layer than Figure 4 because the lower table lookup is shifted by one layer. Furthermore, the execution times for layers change. Some layers now require τ_M instead of τ_R since we expect that the execution of CXOR takes longer than a remote CNOT.

From layers 7–11, we can derive that a controlled table lookup with the zipper construction takes

$$\hat{\tau}_{\text{CTLz}}(2) = 2\tau_R + 3\tau_M \quad (30)$$

cycles. This time does not take into account the copying of input qubits and the additional AND and AND[†] gates in Figure 10a. Together with layer 1, 6, and 12, we derive the recursion

$$\hat{\tau}_{\text{CTLz}}(k) = 2\tau_R + \tau_M + 2\hat{\tau}_{\text{CTLz}}(k - 1) \quad \text{for } k \geq 3, \quad (31)$$

which can be expressed in closed form as

$$\hat{\tau}_{\text{CTLz}}(k) = 2^k(\tau_R + \tau_M) - 2\tau_R - \tau_M \quad \text{for } k \geq 2. \quad (32)$$

Finally, taking into account the overhead from copying input qubits and additional AND and AND[†] gates the cost is

$$\tau_{\text{CTLz}}(k) = 2^k(\tau_R + \tau_M) - \tau_M + O(\sqrt{k}) \quad \text{for } k \geq 2. \quad (33)$$

Here, we account for an $O(\sqrt{k})$ overhead of copying input qubits assuming that they are aligned in a square, as described in the previous section.

Table 2. Comparing expected logical cycles for controlled table lookup (23) with $m = 2$, $\#\text{CCiX} = \min\{k, 2\}$, $\text{CZ} = 2$, and $m = 7$ to numbers obtained from an implementation ($\tau_R = 5$ and $\tau_M = 7$).

k	$\sigma_{\text{CTL}}(k)$	$\tau_{\text{CTL}}(k)$	$\tau'_{\text{CTL}}(k)$	$\tau_{\text{CTLz}}(k)$
1	186	22	22	—
2	292	59	44	41
3	312	133	90	89
4	312	281	214	185
5	332	577	455	377
6	356	1,169	805	761
7	356	2,353	1,812	1,529
8	380	4,721	3,229	3,065

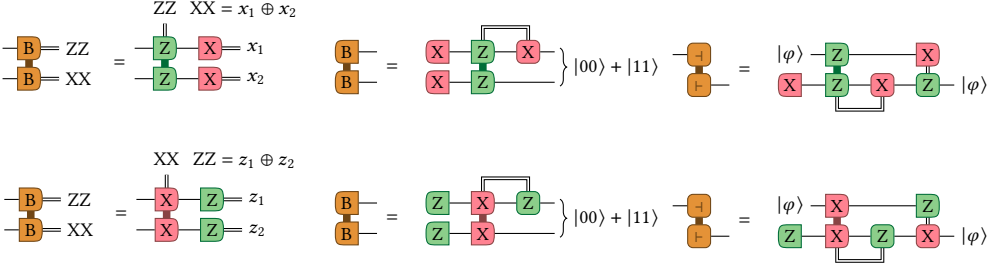


Fig. 12. Axis independent Bell measurement, Bell state preparation and Move operations.

4.2 Experimental results

We have implemented the layout algorithm for a controlled table lookup using the standard construction on k inputs and $K = 2^k$ entries with $\#\text{CCiX} = \min\{2, k\}$ and $\#\text{CZ} = 1$. We choose $m = 7$ and used a simple vertical cat state layout in the implementation of the CXOR gadget. Table 2 lists the results, assuming that preparing $|0\rangle$ and $|+\rangle$ states requires 1 logical cycle, preparing $|S\rangle$ and $|T\rangle$ states requires 5 logical cycles, joint XX and ZZ measurement takes 2 logical cycles, and joint XZ measurement takes 3 logical cycles. Therefore, $\tau_R = 5$ and $\tau_M = 7$. In the implementation there are no strict barriers between the layers which can reduce the effective overall runtime, denoted by $\tau'_{\text{CTL}}(k)$, by up to 1/3 compared to the upper bound. We also list the upper bound for the zipper construction $\tau_{\text{CTLz}}(k)$ for $k \geq 2$. The initialization time, consisting of $|S\rangle$ -state preparation for the CCiX gadgets and the initial preparation stage of the first CCiX execution, is 20 logical cycles and is not included in any of the estimates. Also the initialization time for copying qubits is not included in $\tau_{\text{CTLz}}(k)$.

5 COMMONLY USED GADGETS

We first review an extended set of surface code operations Table 3, which can be implemented as constant depth circuits using a minimal set of surface code operations in Table 1 as explained in this section and supplementary material. Alternatively, many of these operations can be implemented directly in the surface code in a more optimized way.

It is tedious to always have to deal with horizontal and vertical directions for XX and ZZ measurements, so the first step is to introduce axis-independent gadgets of commonly-used operations. In Figure 12, we present axis-independent circuits for Bell measurement, Bell preparation, and the

Table 3. Extended set of surface code operations that can be performed in constant depth. We provide constant depth circuits for all of these operations in the supplementary material.

Operation type	Operation Name(s)
Nearest neighbour adjacent target qubits	Move (Figure 12)
	Prepare Bell (Figure 12)
	Measure Bell (Figure 12)
Remote two-qubit control & target qubits connected by a path	Measure ZZ, Measure XX
	Measure XX & Move, Measure ZZ & Move
	Measure XZ
	CNOT
	Prepare Bell, Measure Bell
	Move
Remote multi-qubit	Prepare x-cat state (Figure 13)
	Prepare z-cat state (Figure 13)
	Fanout (Equation (34))
	Multi-target CNOT
	CXOR (Figure 1)

move operation, which can be used to move the state of a qubit to an ancillary qubit. Their remote versions also have no axis related geometric restrictions.

Remote operations inherit restrictions of their nearest-neighbor versions. Target qubits for joint measurements must be aligned according to the axis. For example, target qubits of remote ZZ measurement must be vertically adjacent to the path of helper qubits connecting the target qubits. Similarly, control qubit of CNOT, CXOR and Multi-target CNOT must be vertically adjacent to the path of helper qubits; all the target qubits must be horizontally adjacent to the path of helper qubits. Measure and Move operations inherit have the same geometric restrictions as applying measure and move sequentially, but have a smaller depth. Remote measure XZ requires a square of qubits along the path mimicking restriction of the local version.

State z-cat can be prepared on a set of vertical segments of a path. Similarly, state x-cat can be prepared on a set of horizontal segments of a path.

The quantum fanout operation achieves the mapping

$$(\alpha |0\rangle + \beta |1\rangle) \otimes |0^{n-1}\rangle \mapsto \alpha |0^n\rangle + \beta |1^n\rangle. \quad (34)$$

This operation can be implemented in constant depth by first creating a z-cat state on the latter $n - 1$ qubits, which results in

$$\frac{\alpha}{\sqrt{2}} |0^n\rangle + \frac{\beta}{\sqrt{2}} |1^n\rangle + \frac{\alpha}{\sqrt{2}} |01^{n-1}\rangle + \frac{\beta}{\sqrt{2}} |10^{n-1}\rangle.$$

By applying a joint ZZ measurement on the first two qubits, one either obtains the expected result when the measurement outcome corresponds to the +1 eigenvalue or, otherwise, an X-correction on each of the last $n - 1$ qubits is needed.

5.1 Switch board construction.

For multiple parallel Bell preparations or teleportations of k qubit pairs $(q_1, q'_{\pi(1)}), \dots, (q_k, q'_{\pi(k)})$ with some arbitrary permutation $\pi \in S_k$, we make use of the following switch board gadgets,

Space-time optimized table lookup

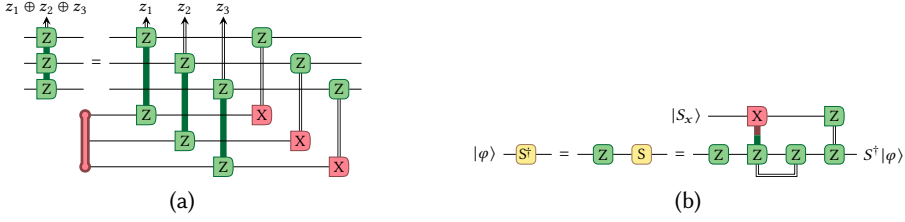


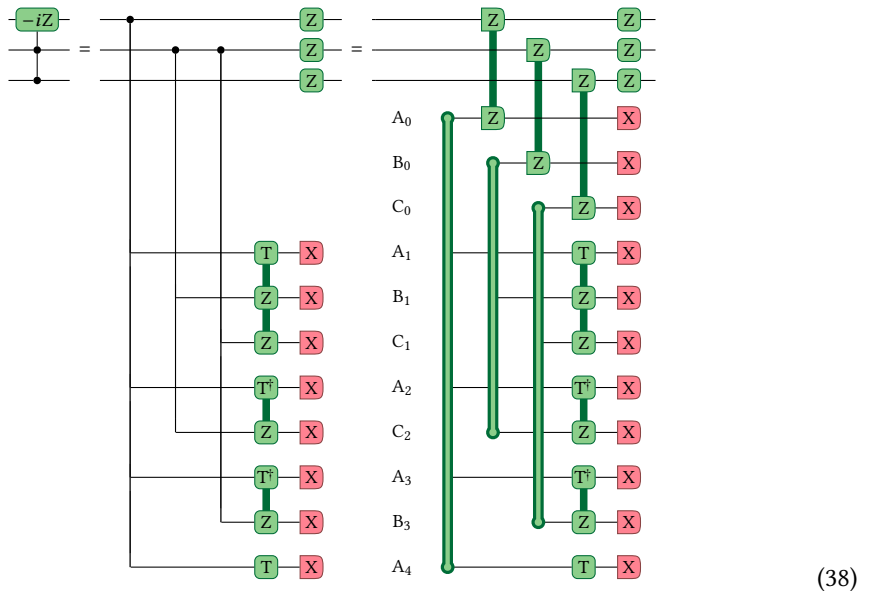
Fig. 14. (a) Multi-qubit joint ZZ measurement using an x-cat state and joint ZZ measurement; (b) S^\dagger gate via $|S_x\rangle$ injection with XZ measurement

Litinski and von Oppen 2018]:

$$\begin{array}{c}
 |T\rangle \\
 \begin{array}{c}
 \text{---} \text{Z} \text{---} \\
 \text{---} \text{Z} \text{---} \\
 \text{---} \text{Z} \text{---}
 \end{array}
 \end{array}
 =
 \begin{array}{c}
 \text{---} \text{Z} \text{---} \\
 \text{---} \text{Z} \text{---} \\
 \text{---} \text{Z} \text{---}
 \end{array}
 \begin{array}{c}
 \text{---} S^\dagger \text{---} \\
 \text{---} X \text{---}
 \end{array}
 \quad (37)$$

If the exponent is negative, e.g., $e^{-i\frac{\pi}{8}(I \otimes Z \otimes Z)}$, the S^\dagger gate is conditionally applied if the result of the multi-qubit joint ZZ measurement is 0.

It is possible to parallelize the execution of all exponential operators by using the fanout gadget and creating four cat-state copies of the target qubit and two cat-state copies for each control qubit. More precisely we create z -cat states on 5 and 3 qubits for the target qubit and each control qubit, respectively, and then using these to both apply the exponential operators as well as connecting the original target and control qubits via joint ZZ measurement. Instead of applying the Z corrections in the exponential operators on qubits A_i , B_i , and C_i as suggested by (37), we collect all X measurement results and compute Z corrections that are directly applied to the control and target qubits of the operation. For example, the Z correction on the target qubit is applied if and only if an odd number of X measurement results is 1:



Note that we can simply transform this doubly-controlled $-iZ$ circuit into a doubly-controlled $-iX$ gadget by conjugating the target line with a Hadamard gate, thereby turning the corresponding joint ZZ measurement and Z correction into a joint XZ measurement and X correction, respectively. The three joint measurements and Pauli corrections in the circuit correspond to those in Figure 7.

The conditional S^\dagger gates in the exponential operators is implemented via $|S_x\rangle$ magic states, where $|S_x\rangle = HS|+\rangle$. We are using the circuit in Figure 14(b) that is derived from Figure 5(a) by conjugating it with Hadamard gates and prepending a Z gate since $S^\dagger = ZS$. It is possible to use joint XZ measurement and CNOT gate to clone an $|S_x\rangle$ state:

(39)

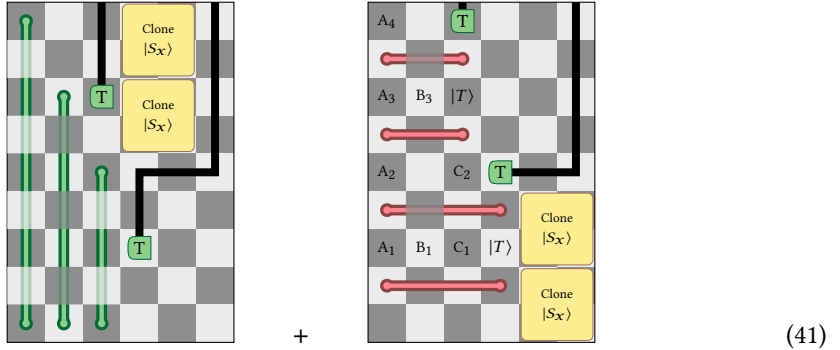
We are making use of this gadget and therefore only need to apply the $|S_x\rangle$ states before executing each CCiX gadget in the table lookup circuit for the first time.

We now have all building blocks to implement (38) on surface code in a 9×6 grid. As illustrated in Figure 7, the implementation consists of a preparation and an execution phase. The location of key qubits in this grid is as follows:

(40)

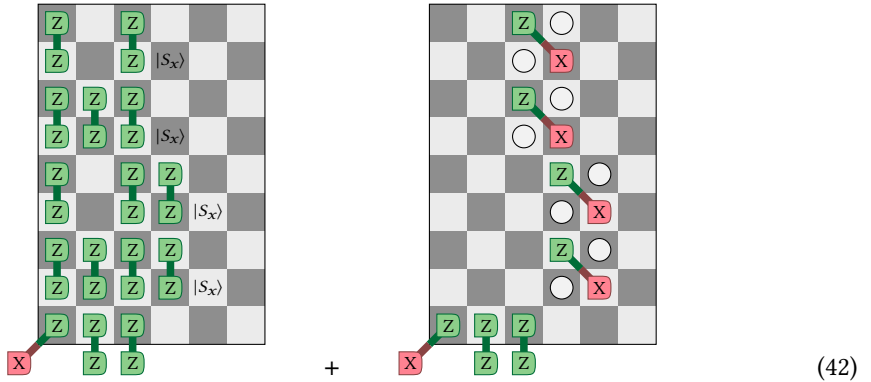
Indices A_i , B_i , and C_i correspond to the cat-state copies in (38). Cells labeled $|T\rangle$ must be prepared in a $|T\rangle$ state in the preparation phase before the exponential operation is executed in the execution phase. Cells labeled $|S_x\rangle$ and highlighted in yellow must be prepared in an $|S_x\rangle$ state once before the CCiX gadget is used for the first time. The other four cells labeled $|S_x\rangle$ will be prepared in an $|S_x\rangle$ state using the cloning gadget in (39) during each preparation stage. Finally, areas outlined in green indicate where z-cat states are prepared, areas outlined in red indicate where exponential operations are executed (see (37)), and areas outlined in yellow indicate where $|S_x\rangle$ states are cloned (see (39)).

The preparation stage consists of the following two steps:



In the first step, fanout qubits are connected via z -cat states. Here we use a more transparent cat state line to indicate holes in the cat state. Also two of the four $|T\rangle$ states are prepared. Note that a $|T\rangle$ state is delivered from the boundary (here from the top). All qubits on the “delivery path,” which is indicated using the black line, must be in a blank state. At the same time, two of the four $|S_x\rangle$ states are cloned. In the second step, the x -cat states used for the multi-qubit joint ZZ measurement (Figure 14) in the exponential operation (see (37)) are prepared and the two remaining $|T\rangle$ and $|S_x\rangle$ states are prepared and cloned, respectively.

The execution stage also consists of two steps:



The three joint measurements in the bottom of the grid are remote measurements and combine the interface qubits A_0 , B_0 , and C_0 (see (38)) with the original target qubit and control qubits, respectively. All other joint measurements are on adjacent qubits. The remote measurements in both steps are the same and their execution time is expected to dominate that of local joint ZZ and XZ measurements.

REFERENCES

- Ryan Babbush, Craig Gidney, Dominic W. Berry, Nathan Wiebe, Jarrod McClean, Alexandru Paler, Austin Fowler, and Hartmut Neven. 2018. Encoding Electronic Spectra in Quantum Circuits with Linear T Complexity. *Physical Review X* 8 (2018), 041015. Issue 4. <https://doi.org/10.1103/PhysRevX.8.041015>
- Hector Bombin, Chris Dawson, Ryan V. Mishmash, Naomi Nickerson, Fernando Pastawski, and Sam Roberts. 2021. Logical blocks for fault-tolerant topological quantum computation. *arXiv preprint arXiv:2112.12160* (2021).
- Sergei Bravyi and Alexei Kitaev. 2005. Universal Quantum Computation with ideal Clifford gates and noisy ancillas. *Physical Review A* 71 (2005), 022316.
- Austin G. Fowler and Craig Gidney. 2019. Low overhead quantum computation using lattice surgery. *arXiv preprint arXiv:1808.06709* (2019).

- Craig Gidney and Martin Ekerå. 2019. How to factor 2048 bit RSA integers in 8 hours using 20 million noisy qubits. *arXiv preprint arXiv:1905.09749* (2019).
- Craig Gidney and Austin G. Fowler. 2019a. Flexible layout of surface code computations using AutoCCZ states. *arXiv preprint arXiv:1905.08916* (2019).
- Craig Gidney and Austin G. Fowler. 2019b. Flexible layout of surface code computations using AutoCCZ states. <https://doi.org/10.48550/ARXIV.1905.08916>
- Thomas Häner, Samuel Jaques, Michael Naehrig, Martin Roetteler, and Mathias Soeken. 2020. Improved Quantum Circuits for Elliptic Curve Discrete Logarithms. In *Int'l Workshop on Post-Quantum Cryptography (Lecture Notes in Computer Science, Vol. 12100)*, Jintai Ding and Jean-Pierre Tillich (Eds.). Springer, 425–444. https://doi.org/10.1007/978-3-030-44223-1_23
- Joonho Lee, Dominic W. Berry, Craig Gidney, William J. Huggins, Jarrod R. McClean, Nathan Wiebe, and Ryan Babbush. 2021. Even More Efficient Quantum Computations of Chemistry Through Tensor Hypercontraction. *PRX Quantum* 2 (Jul 2021), 030305. Issue 3. <https://doi.org/10.1103/PRXQuantum.2.030305>
- Daniel Litinski and Felix von Oppen. 2018. Quantum computing with Majorana fermion codes. *Phys. Rev. B* 97 (May 2018), 205404. Issue 20. <https://doi.org/10.1103/PhysRevB.97.205404>
- Guang Hao Low, Vadym Kliuchnikov, and Luke Schaeffer. 2018. Trading T-gates for dirty qubits in state preparation and unitary synthesis. *arXiv preprint arXiv:1812.00954* (2018).
- Michael A. Nielsen and Isaac L. Chuang. 2000. *Quantum Computation and Quantum Information*. Cambridge University Press.
- David Rosenbaum. 2012. Optimal Quantum Circuits for Nearest-Neighbor Architectures. <https://doi.org/10.48550/ARXIV.1205.0036>
- Peter W. Shor. 1997. Polynomial-Time Algorithms for Prime Factorization and Discrete Logarithms on a Quantum Computer. *SIAM J. Comput.* 26, 5 (1997), 1484–1509. <https://doi.org/10.1137/S0097539795293172>
- Vera von Burg, Guang Hao Low, Thomas Häner, Damian S Steiger, Markus Reiher, Martin Roetteler, and Matthias Troyer. 2021. Quantum computing enhanced computational catalysis. *Physical Review Research* 3, 3 (2021), 033055.

Space-time optimized table lookup

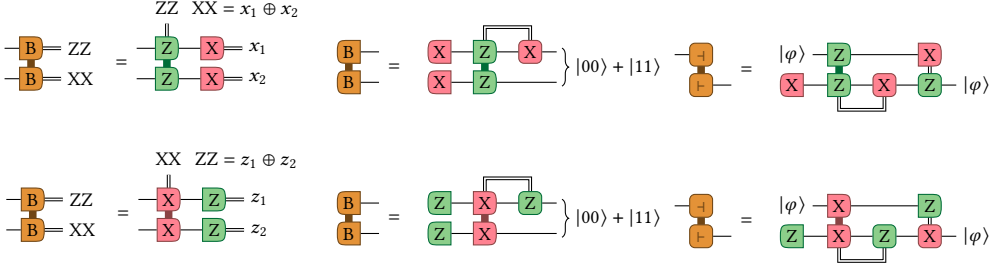


Fig. 15. Axis independent Bell measurement, Bell state preparation and Move operations.

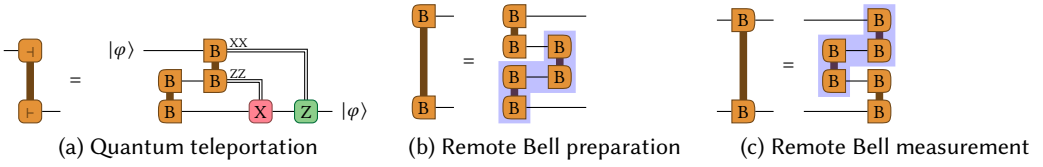


Fig. 16. (a) shows a teleportation circuit composed of Bell state preparation and Bell measurement. (b) and (c) show how to extend the teleportation circuit, highlighted in blue, to construct remote Bell state preparation and Bell measurement.

A EXTENDED SET OF SURFACE CODE OPERATIONS

A.1 Axis-independent operations

It is tedious to always have to deal with horizontal and vertical directions for XX and ZZ measurements, so the first step is to introduce axis-independent gadgets of commonly-used operations. In Figure 15, we present axis-independent circuits for Bell measurement, Bell preparation, and the move operation, which can be used to move the state of a qubit to an ancillary qubit.

A.2 Remote Bell measure and Bell preparation

A remote operation is a constant depth circuit implementing a unitary or a measurement operation between several target qubits connected by a path of ancillary qubits. We make heavy use of such operations in our implementation of table lookup.

Figure 16 shows two examples of simple remote operations derived from a teleportation circuit. The diagram shows Bell preparation and Bell measurement on two qubits that are connected by a path consisting of two ancillary qubits. Replacing local Bell measurement or Bell preparation with the remote version allows us to perform Bell measurements between two arbitrary qubits that are connected by a path of even length in constant depth. To support constant-depth remote Bell measurements with paths of odd lengths, we can make use of the move operation from Figure 15.

A.3 Remote ZZ and XX measurements

Equipped with gadgets for remote Bell measurement and Bell state preparation, we can construct circuits for remote ZZ and XX measurements. As examples for remote joint ZZ measurement, we show three- and four-qubit measurement circuits in Figure 17.

The three-qubit circuit works as follows: The gates in the orange box fan out qubit A to qubit B. The joint ZZ measurement in the blue box is then equivalent to a joint ZZ measurement on qubits A and C. After this joint ZZ measurement, a conditional X-correction could be applied to qubit

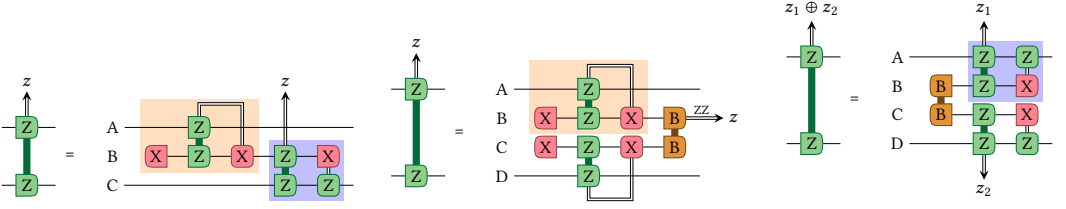


Fig. 17. Remote ZZ measurements on three or four qubits. The orange rectangle highlights “growth along Z direction,” whereas the blue rectangle indicates a “contraction along Z direction.” It is possible that these gadgets can become an optimized operation available directly from surface code.

B in order to ensure that qubits B and C are in a $+1$ -eigenstate of ZZ, allowing us to uncompute qubit B through an X-measurement (and a conditional Z fixup on qubit C). Note, however, that the X-correction on qubit B can be omitted since it commutes with the subsequent X-measurement.

The first four-qubit circuit in Figure 17 fans out qubits A and D to qubits B and C, respectively, before performing a Bell measurement across B and C, which yields the result of the joint ZZ measurement. In contrast, the second four-qubit circuit first establishes a Bell state on qubits B and C. The top joint ZZ measurement then connects the Bell state to qubit A, resulting in qubit A fanned-out across B and C (with a conditional Pauli-X gate on qubits B and C), whereas the bottom joint ZZ measurement can be seen as actually jointly measuring qubits A and D (keeping in mind the potential X-corrections on B and C from the first joint ZZ measurement). The result of the joint ZZ measurement of qubits A and D is thus given by the XOR of the two joint ZZ measurements in the circuit. As was the case for the three-qubit circuit, since—up to conditional X-corrections—qubits A and D are fanned out to qubits B and C, respectively, B and C can be uncomputed using an X-measurement (which commutes with all conditional corrections) and a conditional Z-correction on qubits A and D.

These examples can be extended to a general remote ZZ measurement along an arbitrary path. For example, we get the five-qubit circuit in Figure 18 by inserting the teleportation circuit from Figure 16 into the three-qubit circuit between steps three and four, thus teleporting qubit B to qubit D. Every circuit on k qubits for remote ZZ measurement can be made into circuit on $k + 2$ qubit by replacing two-qubit Bell preparation or measurement circuits with the four-qubit remote Bell preparation or Bell measurement circuits in Figure 16. In Figure 17, we present two circuits on an even number of qubits that we derived from two different four-qubit circuits. Similarly, we derive the circuits for an odd number of qubits from the five-qubit circuit in Figure 18. Possible timing shapes for remote ZZ measurements are shown in Figure 18. Remote XX measurement circuits can be derived from remote ZZ measurement circuits via a simple rule: all Xs need to be replaced by Zs and all Zs need to be replaced by Xs in the circuit. Bell measurements and Bell preparations are left unchanged. Finally, we note that remote ZZ measurement can be performed along an arbitrary path, as long as the target qubits are vertically-adjacent to their ancillary neighbors. Analogously, for remote XX we require the target to be horizontally-adjacent to its ancillary neighbors.

Remote joint measurement with move. Remote joint XX and remote joint ZZ measurements can be constructed on an almost arbitrary path of consecutive adjacent qubits. However, the first pair of qubits and the last pair of qubits must be either horizontally adjacent, in case of a remote XX measurement, or vertically adjacent, in case of a remote ZZ measurement. We will see that gadgets described in the remainder of this section often immediately perform a single qubit measurement on one of the endpoints of a remote joint measurement. In that case we can leverage teleportation to relax the adjacency requirement on one of the endpoints of the remote joint measurement, e.g.,

Space-time optimized table lookup

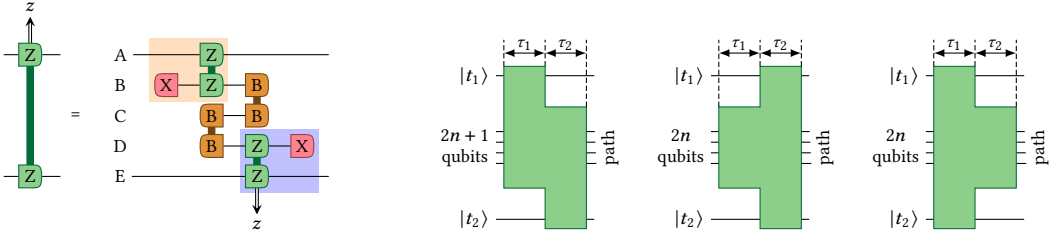


Fig. 18. Remote ZZ measurement on five qubits and timing of multi-qubit remote joint measurement operations. The orange rectangle highlights the “grow along Z direction” gadget, whereas the blue rectangle highlights the “contraction along Z direction” gadget. It is possible that these gadgets can become an optimized operation available directly from surface code. Time τ_1 is the maximum of the times required for Bell state preparation and “growing along Z direction.” Time τ_2 is the maximum of the times required for a Bell measurement and “contraction along Z direction.”

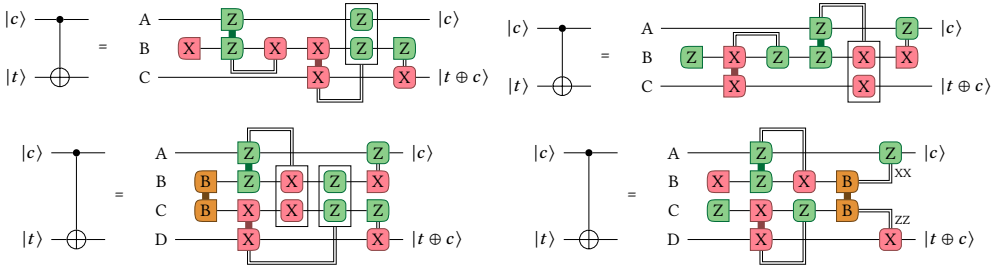


Fig. 19. CNOT on three or four qubits. It is possible that these gadgets can become an optimized operation available directly from surface code.

illustrated for a remote ZZ measurement:

$$\begin{array}{c}
 A \\
 \vdots \\
 B \\
 C
 \end{array}
 \begin{array}{c}
 \text{Z} \\
 \vdots \\
 \text{Z} \\
 \text{Z}
 \end{array}
 \begin{array}{c}
 \text{X} \\
 \vdots \\
 \text{Z} \\
 \text{Z}
 \end{array}
 =
 \begin{array}{c}
 \text{Z} \\
 \vdots \\
 \text{Z} \\
 \text{Z}
 \end{array}
 \begin{array}{c}
 \text{X} \\
 \vdots \\
 \text{Z} \\
 \text{Z}
 \end{array}
 \quad (43)$$

Here, qubits A and B are not adjacent, but qubits B and C are. Note that the joint ZZ measurement can be executed at the same time as the Bell measurements in the teleportation circuit.

A.4 Remote CNOT

Here, we present several constructions for executing a CNOT gate. We start by presenting examples of a CNOT on three and four qubits in Figure 19 (see also [Fowler and Gidney 2019]). The four-qubit circuit can be derived from the three-qubit circuit by replacing the local ZZ measurement with the three-qubit ZZ measurement circuit from Figure 17 and by using the Bell preparation and measurement identities in Figure 16. We get the five-qubit circuits for CNOT in Figure 20 by inserting the teleportation circuit from Figure 16 into the three-qubit circuits for CNOT between steps three and four, thus teleporting qubit D to qubit B. Every circuit on k qubits for remote CNOT can be made into circuit on $k + 2$ qubit by replacing two-qubit Bell preparation or measurement with four qubit remote Bell preparation or Bell measurement circuits in Figure 16. We derive two circuits on even number of qubits from two different four qubit circuits in Figure 19. Similarly we derive odd number of qubit circuits from the five qubit circuits in Figure 20. Possible timing shapes

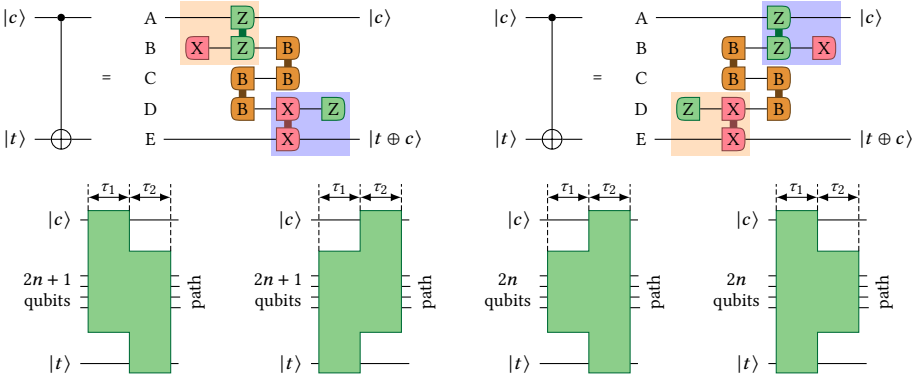


Fig. 20. Remote CNOT gate on five qubits and timing of multi-qubit remote CNOT operations. It is possible that these gadgets can become an optimized operation available directly from surface code. The orange rectangles highlight the “grow along X or Z direction” gadget, whereas the blue rectangles highlight the “contraction along X or Z direction” gadgets. Time τ_1 is the maximum of the times required for Bell state preparation and “growing along X or Z direction.” Time τ_2 is the maximum of the times required for Bell measurement and “contraction along X or Z direction.”

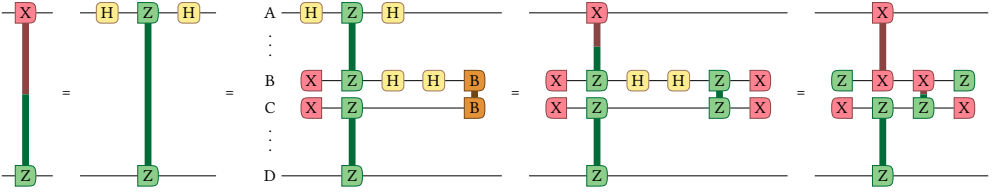


Fig. 21. This example shows how to derive XZ measurement from two remote ZZ measurements combined by Bell measurement. By commuting Hadamard gates we change the topmost remote ZZ measurement and the Bell measurement into a remote XX measurement and an XZ measurement, respectively.

for remote CNOTs are shown in Figure 20. Finally, we note that remote CNOTs can be performed along arbitrary path, as long as the target qubit is horizontally adjacent to its ancillary neighbour and the control qubit is vertically adjacent to its ancillary neighbour.

A.5 Remote XZ measurement

We can construct a remote XZ measurement by replacing the topmost or lowermost joint ZZ measurement with a joint XZ measurement. We can also arbitrarily changing an inner joint ZZ measurement by propagating Hadamard gates through a circuit for remote ZZ measurement. Figure 18 illustrates this based on a circuit that combines two remote ZZ measurements with Bell measurement (see also Fig. 17). The Hadamard gates can be merged into Prepare X and Measure X operations, thereby turning the first remote ZZ measurement into a remote XX measurement and the joint ZZ measurement from the Bell measurement circuit into an XZ measurement.

A.6 Cat state preparation

We use recursive constructions to prepare the states

$$|\text{GHZ}_n\rangle_Z = |\text{GHZ}_n\rangle = \frac{1}{\sqrt{2}}(|0\rangle^{\otimes n} + |1\rangle^{\otimes n}) \quad (44)$$

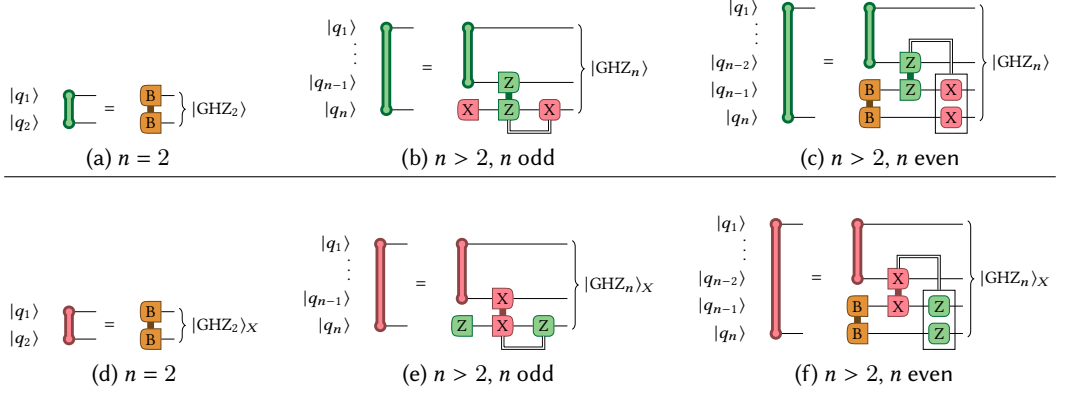


Fig. 22. Cat state preparation on 2 or more vertically adjacent qubits. The cat state preparations used on the right-hand sides are applied to an even number of qubits. Further, consecutive Pauli corrections can be merged by computing the parity of respective measurement results.

and

$$|\text{GHZ}_n\rangle_X = H^{\otimes n} |\text{GHZ}_n\rangle = \frac{1}{\sqrt{2}} (|+\rangle^{\otimes n} + |-\rangle^{\otimes n}) \quad (45)$$

on n vertically adjacent and n horizontally adjacent qubits, respectively. We also refer to these states as z -cat states and x -cat states. Note that

$$|\text{GHZ}_n\rangle_X = \frac{1}{\sqrt{2^{n-1}}} \sum_{\substack{0 \leq i < 2^n \\ vi \bmod 2 = 0}} |i\rangle,$$

i.e., the uniform superposition over all basis states with an even number of 1s in their binary representation.²

We describe our construction for $|\text{GHZ}_n\rangle_Z$ first; the construction for $|\text{GHZ}_n\rangle_X$ is similar. The construction is based on the following decomposition of cat states. For any $n \geq 2$ and $j + k = n$ with $1 \leq j < n$, we have

$$|\text{GHZ}_j\rangle \otimes |\text{GHZ}_k\rangle = \frac{1}{2} (|0^j 0^k\rangle + |0^j 1^k\rangle + |1^j 0^k\rangle + |1^j 1^k\rangle)$$

We can now measure qubit j (the last qubit of the first cat state) and qubit $j + 1$ (the first qubit of the second cat state) using a joint ZZ measurement. If the measurement outcome corresponds to the $+1$ eigenvalue, the resulting state is $|\text{GHZ}_n\rangle$ and otherwise, the resulting state is $\frac{1}{\sqrt{2}} (|0^j 1^k\rangle + |1^j 0^k\rangle)$, which can be transformed into $|\text{GHZ}_n\rangle$ by applying X corrections on either the first j or the last k qubits.

Figure 22(a)–(c) shows our construction based on this decomposition, in which $k \in \{1, 2\}$ such that j is even and X corrections are applied on the last k qubits. The base case is $|\text{GHZ}_2\rangle = \frac{1}{\sqrt{2}} (|00\rangle + |11\rangle)$ when $j = 2$. Since the cat state preparations used in the recursion are applied on an even number of qubits, the resulting circuits have constant depth, with the first layer consisting of Bell state preparations and the second layer consisting of joint ZZ measurements.

Figure 22(d)–(f) shows how to create $|\text{GHZ}_n\rangle_X$ states analogously by replacing X preparation, joint ZZ measurements, and X corrections, by Z preparation, joint XX measurements, and Z corrections, respectively.

²We use vi to refer to the sideways sum of i , i.e., the number of 1s in i 's binary representation.

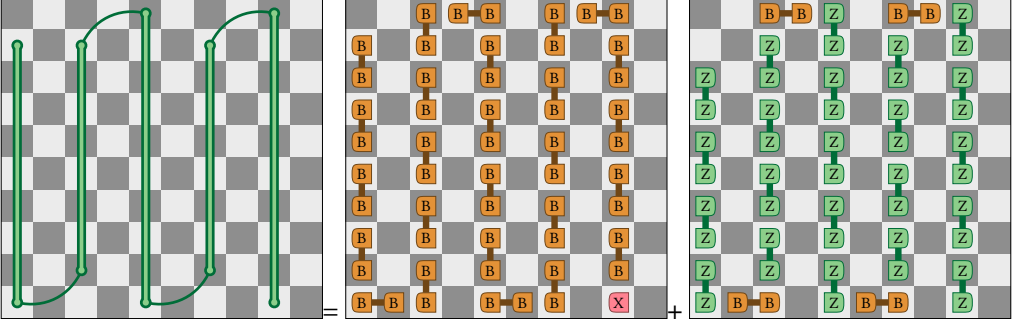


Fig. 23. This cat state along an arbitrary path enables creating a longer z -cat state in a rectangular shape using a snake line pattern.

Cat states with holes. Let $Q = \{q_1, \dots, q_n\}$ be a set of vertically adjacent qubits and let $H = \{h_1, \dots, h_m\} \subseteq Q \setminus \{q_1\}$. Then we can prepare a z -cat state on qubits $Q \setminus H$ by first preparing a z -cat state on Q using the construction above, followed by X measurements on all qubits in H , resulting in measurements r_1, \dots, r_m . We conditionally apply a Z correction on q_1 , if $r_1 \oplus \dots \oplus r_m$ is true. The technique can also be used to prepare an x -cat state on horizontally adjacent qubits, by replacing X measurements and Z corrections with Z measurements and X corrections, respectively.

Cat states on arbitrary paths. We now show how to create a z -cat state on an arbitrary path by leaving holes on segments of horizontally adjacent qubits. The technique works analogously for x -cat states. Contrary to the previous construction, we cannot first create the cat state since joint ZZ measurements can only be applied to vertically adjacent qubits.

Let $Q = (q_1, \dots, q_n)$ be a tuple of qubits, where q_i and q_{i+1} are either vertically or horizontally adjacent. As notation, let $\text{vadj}(q, q')$ and $\text{hadj}(q, q')$ be predicates for the respective adjacency property. We partition Q into

$$q_1 \mid q_2, q_3 \mid q_4, q_5 \mid \dots, \quad (46)$$

where q_n is part of a pair only if n is odd. Then, qubits in Q are part of the cat state if they are not part of a pair, or if they are part of a pair that is vertically adjacent. This is formally captured by the predicate

$$\text{incat}(q_i) = [i = 1] \vee ([n \bmod 2 = 0] \wedge [i = n]) \vee \text{vadj}(q_{2\lfloor \frac{i}{2} \rfloor}, q_{2\lfloor \frac{i}{2} \rfloor + 1}).$$

Let $C = \{q \in Q \mid \text{incat}(q)\}$. Then we can construct a cat state on C in Q with holes $H = Q \setminus C$ using the following procedure:

- (1) Prepare Bell pairs on qubits q_{2i-1} and q_{2i} for $1 \leq i < \frac{n}{2}$. If n is even, prepare qubit q_n in a $|+\rangle$ state.
- (2) For each pair q_i, q_{i+1} as in the partition of (46), do the following based on its adjacency.
 - If $\text{hadj}(q_i, q_{i+1})$, measure the pair of qubit in Bell basis and retrieve two measurement results ZZ and XX (see Fig. 15). Apply a Z correction to q_1 if XX is true, and apply an X correction to q_{i+2} if ZZ is true.
 - If $\text{vadj}(q_i, q_{i+1})$, perform a joint ZZ measurement on q_i and q_{i+1} . If the measurement result is true, apply X corrections to all qubits in $C \cap \{q_1, \dots, q_i\}$.

Figure 23 illustrates an example using this construction in a rectangular shape.

Quantum fanout. The quantum fanout operation achieves the mapping

$$(\alpha |0\rangle + \beta |1\rangle) \otimes |0^{n-1}\rangle \mapsto \alpha |0^n\rangle + \beta |1^n\rangle. \quad (47)$$

Space-time optimized table lookup

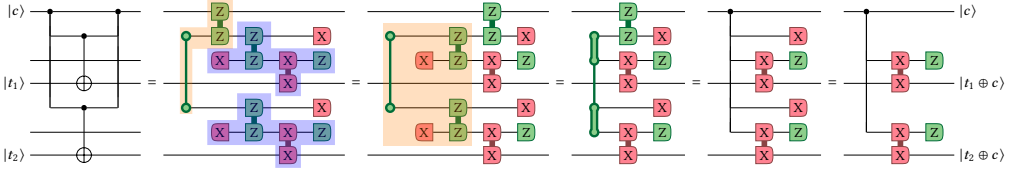


Fig. 24. Derivation of multi-target CNOT based on quantum fanout and CNOT gates.

This operation can be implemented in constant depth by first creating a z-cat state on the latter $n - 1$ qubits, which results in

$$\frac{\alpha}{\sqrt{2}} |0^n\rangle + \frac{\beta}{\sqrt{2}} |1^n\rangle + \frac{\alpha}{\sqrt{2}} |01^{n-1}\rangle + \frac{\beta}{\sqrt{2}} |10^{n-1}\rangle.$$

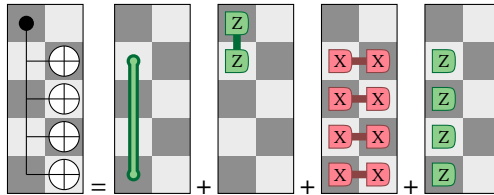
Similarly as done in the decomposition above, by applying a joint ZZ measurement on the first two qubits, one either obtains the expected result when the measurement outcome corresponds to the +1 eigenvalue or, otherwise, an X-correction on each of the last $n - 1$ qubits is needed. Since the additional joint ZZ measurement nicely fits into the layer of joint ZZ measurements for preparing the cat state, the execution time of applying quantum fanout equals the execution time of preparing a cat state.

A.7 Multi-target CNOT

Table lookup relies on a multi-target CNOT to write the output bits into the target qubits. We thus present a resource-efficient implementation (based on low-depth fanout) in terms of our chosen low-level gate set.

We depict a step-by-step derivation of our multi-target CNOT gate in Figure 24. Starting with an abstract quantum circuit using fanout (see Section A.6) and CNOT gates (see Figure 19) on the left-hand side of the figure, we first decompose these operations into surface code primitives. The low-level primitives corresponding to quantum fanout and CNOT gates are highlighted in orange and blue, respectively. In the second step, we move the first joint ZZ measurement past the joint ZZ measurement from the first CNOT gate. We then note that we can extend the two-qubit z-cat state into a four qubit z-cat state (highlighted in orange in the third circuit diagram). This four-qubit cat state together with the joint ZZ measurement on the top two qubits is a quantum fanout operation. Two of the four fanout targets are immediately removed by the X measurement, and therefore the corresponding qubits can be removed altogether, resulting in the final circuit diagram of our multi-target CNOT gate.

In a 2D grid setting, we can use qubits that are horizontally adjacent to cat state qubits as target qubits. Here is an example using a simple vertical cat state:



Note that the joint ZZ measurement and the cat state preparation can be performed simultaneously, resulting in the control qubit being fanned out to all qubits in the left column before the joint XX measurements and the final Z-measurements are applied.